Molecular Hydrogels from Bile Acid Analogues with Neutral Side Chains: Network Architectures and Viscoelastic Properties. Junction Zones, Spherulites, and Crystallites: Phenomenological Aspects of the Gel Metastability

Pierre Terech,*,† Neralagatta M. Sangeetha,‡ and Uday Maitra‡

UMR5819 CEA-CNRS, Université J. Fourier, DRFMC-SI3M-PCM, CEA-Grenoble 17, Rue des Martyrs, 38054 Grenoble Cedex 9, France, and Department of Organic Chemistry, Indian Institute of Science, Bangalore 560 012, India

Received: January 20, 2006; In Final Form: May 10, 2006

Structural and rheological properties of hydrogels made up of neutral bile acid derivatives are studied. Complementary scattering, diffraction, and microscopy techniques provide a precise structural description of the network architecture and its variation as a function of concentration, aging time, composition of the solvent, and type of gelator. Two derivatives (**TH** and **PH**) are considered as presenting favorable scattering features to approach the issue of the competition between gelation versus crystallization. **PH** and **TH** fibers are semirigid cylinders with monodisperse cross-sections (R_0 = 92 and 80 Å, respectively) involving 25 or 12 molecules per cross-sectional repeating unit along the fiber axis. Bundles are cross-links in the networks, and a scattering protocol is developed to determine the nodal and fibrillar fractions in the networks. The effects of alcoholic mixtures, dimethylsulfoxide, and temperature on the network properties are analyzed in terms of the bending modulus of the fibers, the degree of nonaffine character of the regime of deformation, and the dispersion degree of the nodal heterogeneities. It is shown that fibers are semirigid and the scaling laws of the elasticity of the gels with the concentration (exponent $^5/_2$) also support the theoretical context. Head-to-tail molecular arrangements are shown to be similar in the solid and gel phases. Birefringent textures show that spherulitic microdomains coexist in the network texture and are the seeds for a slow crystallization process. The whole pattern might be more general for numerous other self-assembled fibrillar networks found in molecular gels.

1. Introduction

Self-assembled fibrillar networks (SAFINs) are materials attracting increased interest owing to their structural and viscoelastic features that raise fundamental and applied challenges.[1,2] In particular, SAFINs form the solid component of molecular gels made up of low molecular weight organic molecules. The thermal reversibility of the sol-to-gel phase transition and the various thermal equilibria that dictate both the size of the aggregated species and the connectivity of the resulting network are characteristic features of molecular gels that contrast with irreversible covalent networks found in polymeric systems.[3] Molecular hydrogels and organogels can be obtained with a wide range of molecules among which steroid derivatives form a versatile and well-studied class.[1] For instance, cholesterol derivatives have been designed to gelate several organic solvents,[4] and gelators containing the cholesteryl unit appended with various chromophores have been shown to form functional gels.[5] Derivatives of facially amphiphilic bile acids can also gelate aqueous or organic solvents depending on the type of groups appended to the steroid backbone.[6−9] A single example is known for which the genuine steroid skeleton has been modified. This is the exceptional D-homoandrostanyl derivative for which the D ring has been enlarged by the insertion of a nitrogen atom to provide an efficient diamagnetic or paramagnetic organogelator and can be considered as a model system as many aspects of studies (structure, kinetics, stability) have been carried out on this system.[10−12] In other cases, the intact steroid backbone bears variable side chain groups that affect the solvation properties. Solvents ranging from water to organics can be gelated: clearly, ionic functionalities at the side chain lead to the gelation of aqueous solutions, while neutral derivatives with alkyl groups promote gelation of organic solvents. For instance, *N*-isopropyl cholamide[6] and closely related *N*-cholyl amino acid alkyl esters[7] gelate aromatic solvents. Natural bile salts form hydrogels under specific conditions.[13,14] Phosphono analogues[15] of bile acids and several cationic derivatives of bile acids[16] including a tripodal derivative[9] also gelate aqueous solvents.

In this report we elaborate physical properties of hydrogels derived from deoxycholic acid compounds modified by attaching a *neutral hydrophilic* moiety on the side chain so as to modulate the solubility and promote the one-dimensional fibrillar growth in polar aqueous solutions.[17] Structural characterizations of the networks at various length scales are analyzed along with the rheological behaviors for two systems that help addressing the frequently encountered metastability aspect of molecular gels. The issue of the competition between gelation and crystallization is of importance as it clarifies the fundamental differences between a stable thermodynamic phase and a purely kinetic transition state. Theoretically, at the molecular level, gels and crystals may involve identical particle aggregation and dissociation processes followed by a rearrangement step that is either complete (crystallization) or incomplete (nonequilibrium configuration of gels). When the attractive strengths of the

* Author to whom correspondence should be addressed. Phone: +33 4 38 78 59 98. Fax: +33 4 38 78 56 91. E-mail: pierre.terech@cea.fr.
† Université J. Fourier.
‡ Indian Institute of Science.

10.1021/jp060425t CCC: $33.50
Published on Web 07/19/2006

associating individual particles are strong, crystals are formed, and at lower strengths of attraction, gelation can be observed at short time intervals, which may eventually lead to crystal formation at a later time. The theoretical description of the competition between gelation and crystallization is nontrivial, considering that gelation can be considered in a framework of a dynamic and nonergodic transition while crystallization is modeled in a purely thermodynamic approach. The present work provides an example of a self-assembled fibrillar network whose rearrangement and associated gelation as opposed to crystallization could be observed and studied experimentally. Qualitative aspects of the metastability of the hydrogels are presented. The proportion of nodal zones in the network, considered as seeds for the subsequent crystallization process, could be estimated. The structures of the systems studied at different length scales and the related flowing properties support the description. The knowledge of structural conditions favoring the fibrillar growth (based on double nucleation mechanisms)[18] is important to decipher the extremely wide range of lifetimes of molecular gels as lifetime is a determinant factor in evaluating the suitability of these materials for technological applications. The present study globally approaches the gelation phenomenon by associating the structural data at different length scales in relation to the rheological behavior in which the metastable evolution toward crystallization is considered.

2. Experimental Section

Small-angle neutron scattering (SANS) measurements were performed using the D22 spectrometer at Institut Laue Langevin (ILL, Grenoble, France). Deuterated water and dimethylsulfoxide (DMSO) were used (Aldrich) to restrict the level of incoherent scattering of the gels to the contribution due to the gelator molecules themselves. The Q-range available ($Q = 4\pi/\lambda \sin\theta$, λ being the neutron wavelength and θ half of the scattering angle) was $0.001\ \text{Å}^{-1} < Q < 0.6\ \text{Å}^{-1}$. Standard corrections and calibration procedures have been used to proceed with the radial averaging of isotropic two-dimensional arrays of neutron counts collected on the detector (128×128 pixels for an area of 96×96 cm^2 and a pixel size of 0.75×0.75 cm^2).[19]

Rheological measurements used a Haake RS100 controlled stress rheometer with a serrated plate−plate geometry (20 mm diameter, 0.6 mm gap) equipped with a glass cap to limit solvent evaporation at a controlled temperature $T = 20 \pm 0.3$ °C. The gels were formed directly in the gap of the rheometer by introducing the hot sol on the lower plate before bringing the upper plate to the measuring distance. The flowing behaviors illustrated here are an average of at least five trials. The measured yield stress values were independent of the speed of the stress ramp.

Optical micrographs were taken at a magnification of 10× in 1 or 0.5 mm flat quartz cells using an Olympus BX60 microscope (equipped with crossed polarizers). The scanning electron microscope was a Leica 440i apparatus with a LaB_6 emitter, and the solid xerogel samples were coated with a gold layer (∼200−400 Å in thickness). The gel-to-sol melting temperatures (T_{gs}) were estimated by the classical inverted tube method. Fluorescence polarization was measured on a Perkin-Elmer LS-50B luminescence spectrometer. The fluorescence spectra were recorded in 2 or 5 mm square quartz tubes.

The single-crystal X-ray diffraction data were collected on a Bruker AXS single X-ray diffractometer using a SMART APEX CCD detector. The X-ray generator was operated at 50 kV and 35 mA using Mo Kα ($\lambda = 0.7107$ Å) radiation at a sample to detector distance of 6.03 cm. Data were collected with a θ scan with a scan width of 0.3°, and a total of 606 frames per set were collected at three different diffraction angles (0°, 90°, and 180°). Data were reduced and absorption-corrected using the Bruker software package.

The synthesis of the pentahydroxy deoxycholate derivative 2-(3α,12α-dihydroxy-5β-cholan-24-amido)-2-hydroxymethyl-propane-1,3-diol (**PH-DC**) was accomplished by stirring a solution of methyl 7-deoxycholate (2.02 g, 5 mmol) in DMSO (6 mL) with 2-amino-2-hydroxymethyl-1,3-propanediol (850 mg, 7 mmol) and K_2CO_3 (830 mg, 6 mmol) at room temperature. After 14 h, the solution was filtered, and the solvent was removed. The crude product was purified on a silica column using 5−20% EtOH/$CHCl_3$ as the eluent to yield (69%) 1.7 g of the pure product (mp 205−206 °C). α_D:[25] 38.0 (c 2.0, EtOH). IR (neat, cm^{-1}): 3423, 2935, 2864, 1635, 1042. ^{1}H NMR (300 MHz, DMSO-d_6) δ: 0.57 (s, 3H), 0.82 (s, 3H), 0.89 (d, $J = 6$ Hz, 3H), 0.95−2.16 (m, steroidal CH, CH_2), 3.35 (m, 1H), 3.77 (br s, 1H), 4.2 (d, $J = 4$ Hz, 1H), 4.55 (d, $J = 4$ Hz, 1H), 4.82 (t, $J = 5.7$ Hz, 3H), 7.09 (s, 1H). ^{13}C NMR (75 MHz, DMSO-d_6) δ: 12.61, 17.30, 23.26, 23.71, 26.30, 27.17, 27.43, 28.77, 30.33, 31.82, 33.13, 34.00, 35.25, 35.30, 35.87, 36.38, 41.80, 46.18, 46.38, 47.65, 61.03, 62.36, 70.22, 71.31, 174.79. FAB-MS: Calcd for $C_{28}H_{49}NO$ + H, 496.3634. Found, 496.3638. Anal. Calcd for $C_{28}H_{49}NO_6 \cdot 2H_2O$: C, 63.25; H, 10.04; N, 2.63. Found: C, 63.41; H, 9.77; N, 2.98.

The synthesis of the tetrahydroxy deoxycholate derivative 2-(3α,12α-dihydroxy-5β-cholan-24-amido)-2-methyl-propane-1,3-diol (**TH-DC**) was done by heating a solution of methyldeoxycholate (250 mg, 0.615 mmol) in DMSO (2 mL) with 2-amino-2-methyl-1,3-propane diol (122 mg, 1.16 mmol) and K_2CO_3 (109 mg, 0.79 mmol) heated at 70 °C. After 30 h, the solution was filtered, and the solvent was removed. The crude product was purified on a silica column using 10−20% EtOH/$CHCl_3$ as the eluent to yield (67%) 197 mg of the pure product (mp 163−164 °C). α_D:[25] 44.4 (EtOH, c 2.07%). IR (KBr, cm^{-1}): 3385, 2937, 2864, 1633, 1538, 1448, 1377, 1256, 1170, 1044. ^{1}H NMR (300 MHz, DMSO-d_6) δ: 0.59 (s,3H), 0.84 (s, 3H), 0.91 (d, $J = 6$ Hz, 3H), 0.99−2.16 (m, steroidal CH and CH_2), 1.09 (s, 3H), 3.78 (s, 1H), 4.17 (d, $J = 4.2$ Hz, 1H), 4.48 (d, $J = 3.9$ Hz, 1H), 4.84 (t, $J = 5.4$ Hz, 2H), 7.12 (s, 1H). ^{13}C NMR (75 MHz, DMSO-d_6) δ: 12.46, 17.18, 18.86, 23.12, 23.57, 26.17, 27.06, 27.28, 28.66, 30.26, 31.72, 32.99, 33.14, 33.86, 35.11, 35.20, 35.73, 36.32, 41.69, 46.05, 46.25, 47.51, 58.40, 64.26, 70.06, 71.13, 173.74. HRMS TOF-MS ES+: Calcd for (M^+ + Na), 502.3526. Found, 502.3531. Anal. Calcd for $C_{28}H_{49}NO_5 \cdot H_2O$: C, 67.57; H, 10.33; N, 2.81. Found: C, 67.27; H, 10.32; N, 2.35.

3. Results, Analysis, and Discussions

3.1. Gelation. The gels were prepared by dissolving the gelator in varying amounts of polar cosolvents (MeOH, EtOH, DMSO, dimethylformamide (DMF), AcOH, etc.) before dilution with water. With **PH** in ethanol, added water gives either a clear solution or a cloudy mixture depending on the gelator concentration. Upon inspection, these mixtures slowly developed small globular gel aggregates that grew with time until they occupied the entire volume of the liquid. In cases where the cloudy solution is heated to homogeneity and allowed to cool naturally to room temperature (25 °C), the solution developed cloudiness (an indication of supersaturation) before gelation occurred. **PH** forms stable gels in 10−30% MeOH/H_2O, 10−25% EtOH/H_2O, 30% DMSO/H_2O, 10−20% AcOH/H_2O, and 20% DMF/H_2O at 0.2% w/v and produces homogeneous solutions for higher amounts of the cosolvent. Gels thus prepared (except in AcOH/

CHART 1

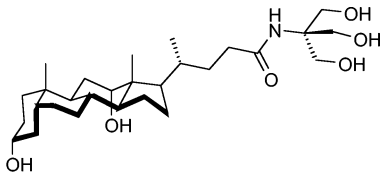

PH

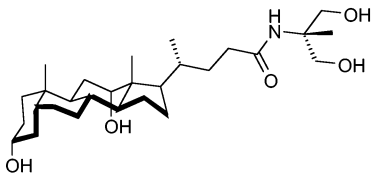

TH

H_2O) are stable for several months. **TH** forms gels in 10−30% MeOH/H_2O, 10−25% EtOH/H_2O, 30−80% DMSO/H_2O (almost an organogel), and 20% DMF/H_2O at 0.2% w/v and produced homogeneous solutions in higher percentages of the organic solvents. **TH** gels in EtOH/H_2O, MeOH/H_2O, and AcOH/H_2O are unstable and phase-separate to give crystals in 2−24 h. Gels of DMSO/H_2O are more stable and can be preserved in sealed tubes for several days. The tendency to phase-separate into fibrous crystals is higher when the gelator concentrations are high. The comparison of the gelation phenomenology of **PH** and **TH** gels is an instructive step before a more refined analysis of the gelation versus crystallization competition is conducted. The analysis focuses on **PH-DC** (pentahydroxy deoxycholic derivative) and **TH-DC** (tetrahydroxy deoxycholic derivative) forming transparent gels in a DMSO/H_2O mixture (40% v/v) within a concentration range of 0.4−2.5% w/v (Chart 1). For such a solvent composition, the potential for solvent evaporation is advantageously low as compared to gels in low boiling point alcoholic solvents. Moreover, at concentrations above 2.5% w/v, gels undergo a relatively rapid phase separation process that offers an opportunity for studying the metastability aspects of such SAFINs.

3.2. Nanostructures in the Gel Network. Small-angle neutron scattering experiments are used to characterize the structures of the aggregates in the gel networks. In particular, the scattering curves demonstrate that the **PH-DC** and **TH-DC** swollen gels are made up of rigid fibers (i.e., the modeling does not require the involvement of the persistence length l_p of the fibers). The scattering curves present three angular parts (Figure 1): the low-Q region I ($Q < 0.01$ Å^{-1}), the intermediate-Q region II ($0.01 < Q < 0.3$ Å^{-1}), and the large-Q region III ($Q > 0.3$ Å^{-1}). Domain I contains the information related to large-scale heterogeneities in the system. The description of the scattering in region I can be made either (i) in terms of interfacial scattering of large species, (ii) using an exponential distribution of the heterogeneities,[20] or (iii) by assuming that the heterogeneities are fractal structures that exhibit self-similarity in a given spatial range.[21] For instance, with mass fractals, the fractal dimension d_f is defined as the exponent of the linear dimension R according to the relation $M(R) \sim (R/r_0)^{df}$ (M being the mass and r_0 the gauge of the measurement) corresponding to a simple scattering function of the type $S(Q) \sim Q^{-df}$.[22] Experimentally, in region I, for the two gels, the exponent of the power law describing the intensity decay varies from ca. 1.5 to 3.9 as the concentration is increased. The profiles appear more sigmoidlike than straight as expected for fractals. This pattern rather supports the presence of large heterogeneities with an asymptotic scattering decay of the type $I \propto Q^{-4}$ expected for large nodal

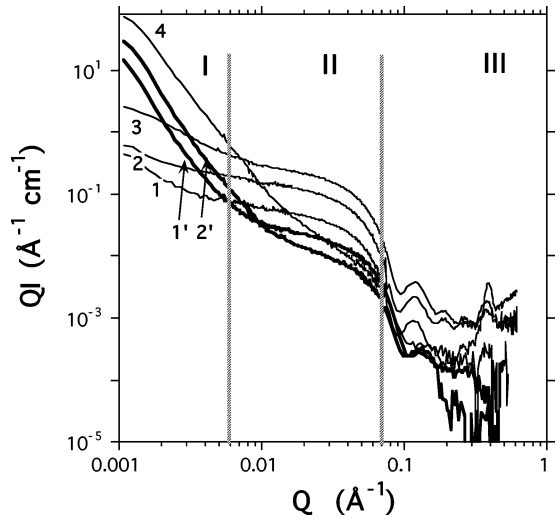

Figure 1. SANS curves of **PH** and **TH** hydrogels represented in a Q vs I plot, facilitating the identification of fibrillar species. Three angular domains I, II, and III are distinguished for the analysis (see text). **PH** hydrogels: **1** ($C = 0.00323$ g cm^{-3}, DMSO/$D_2O = 0.4$), **2** ($C = 0.0075$ g cm^{-3}, DMSO/$D_2O = 0.4$), **3** ($C = 0.0132$ g cm^{-3}, DMSO/$D_2O = 0.4$), **4** ($C = 0.0167$ g cm^{-3}, $CD_3OD/D_2O = 0.2$). **TH** hydrogels: **1′** ($C = 0.0057$ g cm^{-3}, DMSO/$D_2O = 0.5$), **2′** ($C = 0.01268$ g cm^{-3}, DMSO/$D_2O = 1$).

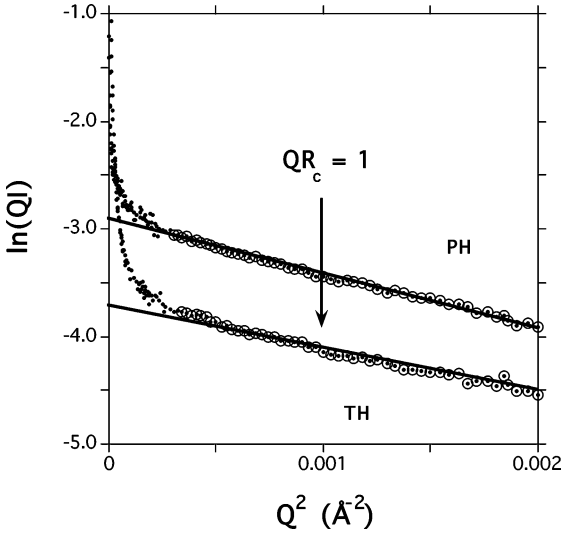

Figure 2. Guinier plots for **PH** ($C = 0.00323$ g cm^{-3}, DMSO/$D_2O = 0.4$) and **TH** ($C = 0.0057$ g cm^{-3}, DMSO/$D_2O = 0.5$) hydrogels. Straight lines are best fits of ln(QI) vs Q^2 fits using $I(Q) = \phi(\pi/Q)\Delta\rho^2\pi r^2 \exp(-Q^2R^2/4)$. The low-$Q$ sharp upturn is attributable to the network heterogeneities (domain I). See also Table 1.

zones in SAFINs.[23] This first hand information is important for the subsequent step analyzing the composition of the gel network made up of fibers and junction zones. Domain II shows a Q^{-1} decay characterizing the one-dimensional character of the aggregates (see caption to Figure 2). The cross-sectional radius of gyration of the fibers can be extracted from ln(QI) versus Q^2 plots (known as a "Guinier plot" for rodlike scatterers) as shown in Figure 2. A linear variation is observed in the intermediate Q-range ($Q^2 < 0.001$ Å^{-2}) that extends beyond the validity condition $QR_C = 1$ (R_c being the cross-sectional radius of gyration of the fibers), and its slope is related to the geometrical radius R_0 of cylindrical fibers ($R_c = R_0/\sqrt{2}$). The intense extra scattering contribution arising from large-scale heterogeneities of the network (domain I) also appears naturally at the innermost part of the plot of Figure 2. Domain III presents

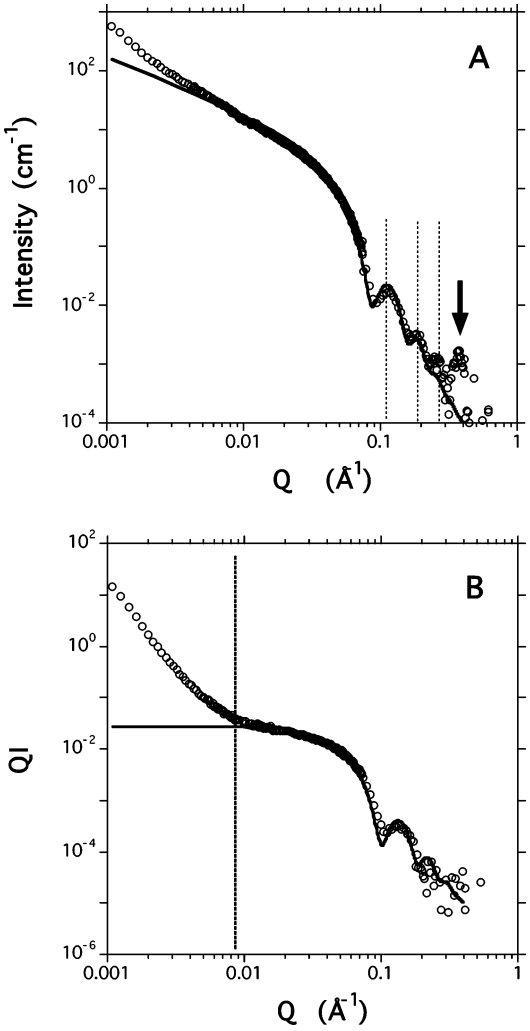

Figure 3. Example of the agreement obtained in domain II with the theoretical form factor for rigid, homogeneous cylindrical fibers $I(Q) = (\pi L/Q)[\pi R^2 \Delta\rho(2J_1(QR)/QR)]^2$. (A) **PH** gel, $C = 0.0075$ g cm^{-3}, DMSO/$D_2O = 0.4$, $R_0 = 46$ Å, ϵ (radial dispersity) $= 0.1$. Three dotted vertical bars indicate the form-factor oscillations. The bold arrow points at Bragg peak at $Q = 0.379$ Å^{-1}. **(**B) Cross-sectional intensity vs Q. **TH** gel, $C = 0.0057$ g cm^{-3}, DMSO/$D_2O = 0.5$, $R_0 = 39.6$ Å, $\epsilon = 0.1$.

form-factor oscillations arising due to the monodisperse cross-sections of the gel fibers. Bragg peak(s) can also be occasionally observed (curves 1, 2, 3, and 4 for **PH** gels in Figure 1) and characterize the molecular arrangement in the fibers and their bundles. Interestingly, **TH** gels do not exhibit Bragg peaks in this Q-range, and the observation suggests that their networks connect more amorphous nodal zones despite their pronounced ability to phase-separate into crystals as compared to **PH** gels (subsection 3.1). Figure 3 shows that the theoretical scattering function (see caption) for long and rigid cylinders satisfactorily reproduces the scattering profile in domains II and III (except the Bragg peak). Figure 3A illustrates the quality of the I versus Q agreement for a **PH** gel consisting of fibers of diameter $D =$ 92 Å and a radial definition monodisperse enough to exhibit up to three form-factor oscillations (in this representation) preceding a Bragg peak. Similarly, Figure 3B shows the QI versus Q situation for a **TH** gel for which fibers of diameter $D \approx 79$ Å satisfactorily reproduce the scattering behavior. The QI versus Q representation ("Holtzer plot") is convenient to visualize the separation of the form-factor contribution for fibers with its horizontal asymptotic signature from the intense signal

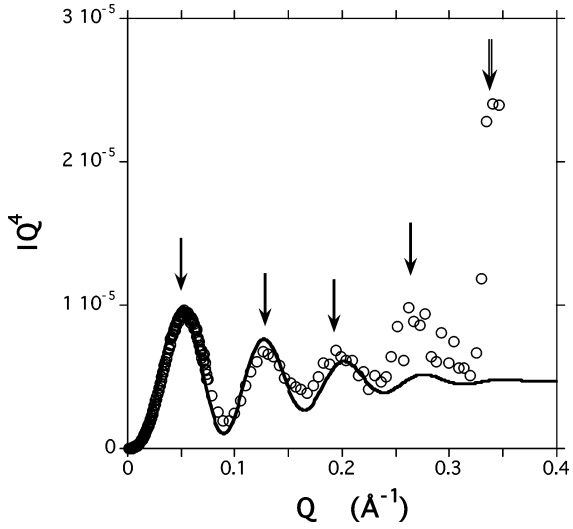

Figure 4. Porod's plot demonstrating the high level of monodispersity of the homogeneous cross-sections of fibers forming the **PH** hydrogel ($C = 0.0132$ g cm^{-3}, DMSO/$D_2O = 0.4$, $R_0 = 44.5$ Å, $\epsilon = 0.1$). Four arrows point at the form-factor oscillations; the double arrows indicate the Bragg peak at $Q = 0.379$ Å^{-1}.

accounting for heterogeneities (Q-domain I, vertical bar). The high degree of radial monodispersity of **PH** fibers is also evident from the observation of up to four well reproduced oscillations in a IQ^4 versus Q representation (Porod's plot) (Figure 4). Under similar conditions, **TH-DC** fibers exhibit only two oscillations, but it is not sufficient to conclude that the sections are less monodisperse, since these oscillations are narrower and the corresponding scattering signal attributable to the cross-sections is rejected at larger Q-values. Table 1 collects the structural parameters extracted from the Guinier's plots and from the fit of the scattering curve in domains II and III for the six gels at different concentrations. It is clear from Figure 1 that there is a drastic change of the intensity profile in Q-domain I when the deuterated cosolvent DMSO is replaced by deuterated ethanol. The Bragg peak for **PH** gels is in the range 0.376 Å^{-1} $\leq Q \leq$ 0.389 Å^{-1} and corresponds to reticular planes periodically spaced by 16.15 Å $\leq \langle d \rangle \leq$ 16.7 Å, the molecular length l_{mol}. **PH-DC** molecules are thus stacked head-to-tail in the cylindrical fibers of the gel network, and the diameter results from the radial assembly of a multiple n of **PH** molecules ($5.5 \leq n = 2R_0/l_{mol} \leq 5.7$). The concentration and type of cosolvent can affect the extensional degree of the gelator molecules within the sections of fibers and/or the mosaicity of more or less compact bundles,[24] and this can account for variations in the position of the broad Bragg peak. At this stage of analysis, the most striking structural features observed for **PH** and **TH** hydrogels are (i) the high monodispersity of the cross-sections of rigid cylindrical fibers, (ii) the fixed number of molecules per diameter in the cross-sections, and (iii) the scattering profiles (**PH** hydrogels) with a favorable Q-separation between the form factor of thin fibers and the intense extra scattering attributable to nodal zones where fibers merge. The latter motivates a deeper analysis to estimate the volume fraction of the cross-links in the network. The nodal scattering component is enhanced by an increase of the gelator concentration (or change of solvent type; see curve 4 in Figure 1), and its variation is assumed to be parallel with the fraction of heterogeneities. The scattering signal in domain I−II evolves from an almost pure form-factor contribution (curve 1 in Figure 1 or 3) to a Q^{-4} decay, and concomitantly, a Bragg peak grows at $Q \approx 0.39$ Å^{-1}. Interestingly, **TH** gels exhibit a Q^{-4} intensity decay in domain I even

TABLE 1: Structural Parameters Extracted from Guinier's Plots,[a] the Fit of the Scattering Profile,[b] the Invariant Procedure for the Estimation of the Fraction of Nodes ϕ_n and the Number of Aggregated Molecules per Angstrom of Fiber n_L[c,d]

system	C (g cm^{-3})	solvent	R(fit) (Å)	slope	R(Guinier) (Å)	$\ln(QI)_0$ (Å^{-1} cm^{-1})	n_L (mol Å^{-1})	ϕ_n
PH	0.00323	DMSO/D_2O = 0.4	45.1	508.53	45.1	−2.908	5.1	0.14
PH	0.0075	DMSO/D_2O = 0.4	46	567.64	47.7	−1.8846	5.1	0.18
PH	0.0132	DMSO/D_2O = 0.4	46	528.75	46.0	−1.3114	5.3	0.25
PH	0.0167	CD_3OD/D_2O = 0.2	38.6	373.34	38.6	−4.0301	2.5	0.94
TH	0.0057	DMSO/D_2O = 0.5	39.6	391.29	39.6			0.29
TH	0.01268	DMSO/D_2O = 0.5	40.2	405	40.2			0.67

[a] Slope α, $r_0 = 2\sqrt{\alpha}$; extrapolation at $Q \rightarrow 0$, $(QI)_0$. [b] R(fit). [c] $n_L = 10^3 N((QI)_0/\pi M^2(C - C_g)\phi_f(\overline{\Delta b})^2)$. [d] The specific neutron scattering contrast is $\overline{\Delta b} = -4.6488 \times 10^{10}$ cm g^{-1} for **PH** in DMSO/D_2O mixture, -5.3706×10^{10}cm g^{-1} in CD_3CD_2OD/D_2O mixture, and -4.5597×10^{10} cm g^{-1} for **TH** gels in DMSO/D_2O mixture. The effective concentration involved in the fibers takes into account the minimum aggregation concentration $C_g \approx 0.002$ mM $\equiv 0.001$ g cm^{-3} (for **PH**) and the fraction of fibers in the network ϕ_f. n_L was not estimated for **TH** gels since C_g is unknown and the high proportion of nodes in a phase-separating system makes the determination too hazardous.

at low concentration, implying the presence of a larger fraction of rather amorphous heterogeneities. This observation is consistent with the one made on the enhanced metastability of **TH** gels at low gelator concentration (subsection 3.1). The distinct phenomenology between **PH** and **TH** gels is symptomatic of the complexity of the SAFINs. Nevertheless, the pattern for **PH** hydrogels is favorable for the elaboration of a SANS methodology evaluating the fraction of aggregated gelator molecules in the nodal zones.

The scattering invariant INV, defined as the integral in eq 1, is related to the mean-square fluctuation of the neutron scattering length density ($\Delta\rho$) over the volume of the scatterers of volume fraction ϕ and volume V

$$\mathrm{INV} = \int_0^\infty Q^2 I(Q)\, \mathrm{d}Q = 2\pi^2 V\gamma(0) = (\Delta\rho)^2\phi(1-\phi)2\pi^2 \quad (1)$$

The correlation function $\gamma(r)$ is the average of the product of two fluctuations at a distance r. As long as the scattering profile can be reproduced by the sum of a form-factor and a Debye−Büeche-type component[20] for randomly dispersed heterogeneities, the invariant can also be split into two contributions INV_f (for fibrillar structures) and INV_n (for the contribution from the nodes). INV_f is calculated directly from the best fit to the theoretical scattering function for cylinders (see caption to Figure 3), and INV_n is deduced from the integration of the whole experimental scattering signal (INV) according to $INV_n = INV - INV_f$. It is assumed that there is no significant neutron contrast difference between aggregated gelators in the fibers and those in the nodal zones since it is reasonable to envision the latter as rather compact bundles of fibers. Equation 1 is thus used to extract the variation of the nodal volume fraction ϕ_n in the network with the gelator concentration (Figure 5). The Bragg peak's width, ϕ_n, and amplitude follow regular ascending ramps with a sharp singularity corresponding to a change of cosolvent from DMSO to CD_3CD_2OD. The sharpening of the Bragg peak is correlated with its amplitude and is associated with a corresponding increase of the size of the ordered domain. The nodal heterogeneities in the gel networks possess correlated scattering signatures in the extreme parts of the scattering curves. The variation of the node fraction increases regularly with the global concentration: In DMSO/D_2O, $\phi_n = 0.04 + 17.4C_0$. Actually, the effective concentration involved in the fibers and nodes is only $(C_0 - C_g)$ in a supersaturated state at a given temperature (where C_0 and C_g are the total gelator concentration and the actual concentration involved in network formation, respectively). The gelation concentration C_g has been estimated from fluorescence probing studies using pyrene as a fluorophore in **PH** 20% EtOH/H_2O gels. The fluorescence and the anisotropy

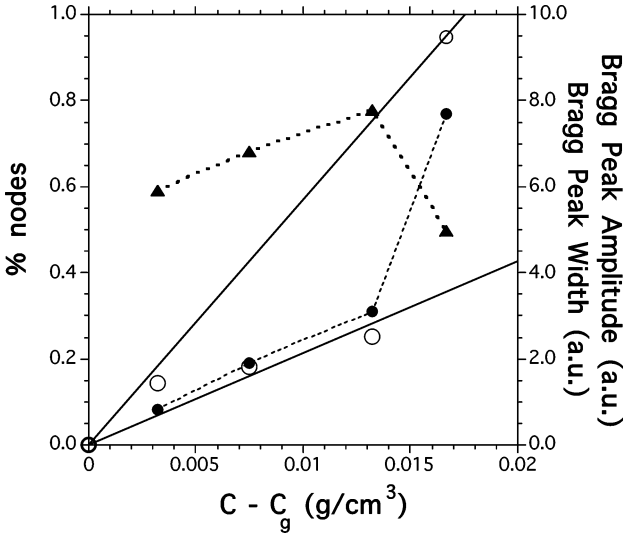

Figure 5. Variation of the fraction of nodes (○), Bragg peak amplitude (●), and width (▲) as a function of the **PH** concentration in hydrogels of Figure 1. The first three data points correspond to the DMSO/D_2O solvent while the fourth one is for CD_3CD_2OD/D_2O. Dotted connecting lines between the data points are guides to the eye. The two full straight lines are theoretical variations for the node fraction in DMSO/D_2O ($\phi_n = 21.4\,(C - C_g)$) and CD_3CD_2OD/D_2O ($\phi_n = 56.9\,(C - C_g)$).

of the dissolved fluorophore measured as a function of **PH** concentration show a single inflection at 2 mM (C_g) that matches with the gelation threshold estimated by visual inspection (not shown). Figure 5 shows the corrected variations that assume that at $C - C_g = 0$, $\phi_n = 0$. It characterizes the crystalline-like character of the gel in CD_3CD_2OD/D_2O that is almost 3 times that in DMSO/D_2O. The profiles demonstrate that the number density of heterogeneities of a given size corresponding to Q-domain I ($\langle d\rangle \approx 2\pi/0.01 \approx 600$ Å) increases with C. At a similar gelator concentration, the change of cosolvent from DMSO to CD_3CD_2OD induces a sharp increase of the size of the organized domains. Assuming that the crystalline-like character of a SAFIN is related to the proportion and size of domains organized on a molecular scale, the present phenomenology suggests that the energetic (enthalpic) term of the free energy of the network overwhelms the entropic one (favoring the number density of fibers) to generate an architecture dominated by large-sized domains or bundles (revealed by the related Q^{-4} scattering behavior).

It is interesting to schematize the **PH** SAFIN to estimate the mesh size ξ in an ideal network of stiff fibers distributed in a cubic skeleton. Thus, ξ can reduce to $\xi \approx D\sqrt{(\pi/\phi)}$ where D is the transverse size of the fibrillar species. At $C \approx 0.013$ g cm^{-3} (third data point of Figure 5), the nodal fraction is $\phi_n = 0.25$,

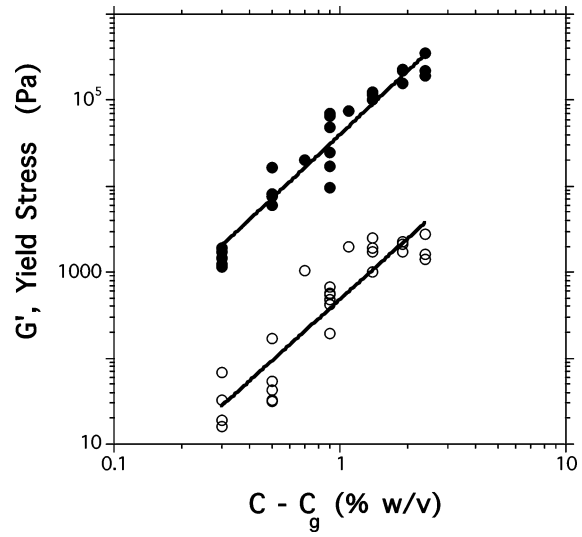

Figure 6. Scaling laws as a function of the effective concentration for the storage modulus (exponent = 2.5) and yield stress (exponent = 2.4) of **PH** hydrogels.

the fraction of gelators in the fibers is $\phi_f = 0.75$, and the equivalent mesh size at $\phi = 0.75C$ is on the order of ca. 1600 Å. This distance is large since the percentage of nodes is significant (25%) and the fibers rather thin ($2R = 92$ Å), but scanning electron micrographs will show (vide infra) that, nevertheless, it is comparable or smaller than a rigidity distance characteristic of the **PH** fibers. The cubic distribution of fibers is certainly an oversimplified hypothesis using the isotropic assumption whose validity at all length scales ($\geq \xi$) is questionable. Birefringent textures are observed in these gels (vide infra) and reveal that locally a significant orientational order prevails in microdomains of the network architecture. At a constant quantity of rods, a more hexagonally structured assembly would significantly decrease the mesh size by a factor of ca. $^1/_3$. In the idealized example, the resulting mesh size would reduce to ca. 500 Å and would definitely place **PH** SAFIN in the class of networks for which the persistence length and contour lengths are significantly larger than the mean distance between cross-links, and this will have profound consequences on the rheological properties of the systems.

3.3. Rheological Properties. PH and **TH** gels exhibit rheological profiles (i.e., G', G'' versus frequency of the applied stress) typical of soft viscoelastic solids.[16] Elastic shear and loss moduli are almost independent of the frequency ($G' \propto C^{0.031}$ and $G' \propto C^{0.066}$ for **PH** and **TH** gels, respectively) and $G'/G'' \approx 10$ and 15 for **TH** and **PH,** respectively (not shown). At comparable concentrations, **PH** gels are mechanically stronger than **TH** gels and have an extended linear viscoelastic domain. Interestingly, the linear regime of deformations is restricted to small levels of strain of about 0.01 for **PH** in 40% DMSO/H_2O ($C = 1.5\%$ w/v) and to smaller strains (~0.005) for **TH** gels (1.25% w/v in 50% w/v DMSO/H_2O). No significant variation of the linear regime of deformation with the concentration is observed (**PH** gels in 40% DMSO/H_2O) excluding the analysis of the rheological properties in the context of colloidal gels.[25]

Variation of both G' and σ^* with the effective concentration ($C - C_g$) follow power laws (Figure 6). For **PH** gels (40% DMSO/H_2O), the exponent for the storage modulus is 2.5 ($r = 0.91$) while that for the yield stress is 2.4 ($r = 0.80$). Such power laws are useful to identify the most suitable theoretical context accounting for the mechanism of deformations in such networks. It has already been shown that most SAFINs in organo- and hydromolecular gels exhibit a scaling exponent of G', σ^* versus

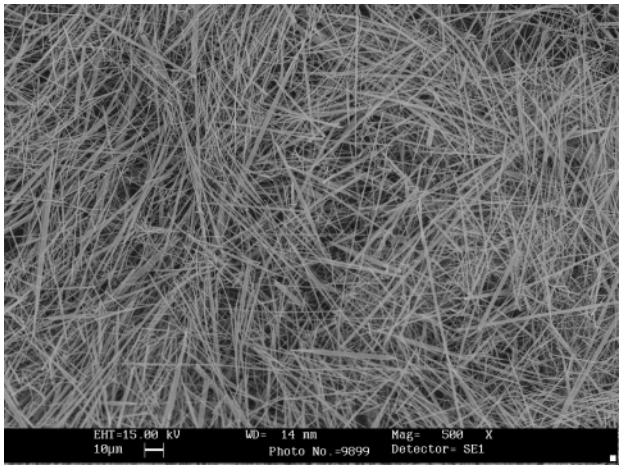

Figure 7. Scanning electron micrograph of a **PH** xerogel obtained from a 20% MeOH/H_2O gel. The view presents similarities with the "Mikado model" of a two-dimensional random network of rigid rods.[38]

concentration close to 2,[26,27] which can be accounted for in the theoretical context of rigid energetic networks of fibers[28] or cellular solids.[29,30] It is interesting to note that an alternative context involving the packing of fractal flocs in colloidal gels[25,31] has already been evoked, which was also discussed in the concentrated regime of particular cationic bile acid hydrogels.[16] The analysis relied on the variation of the viscoelastic linearity with the gelator concentration and the fractal dimension of the floc (and its effective backbone). No such variation in the linearity domain is experimentally observed with **PH** and **TH** hydrogels, and small-angle neutron scattering experiments also provide useful clues. In particular, the low-Q decay of the scattering component assigned to the heterogeneities (or nodal zones) in the gels does not confirm the existence of a fractal signature of the type $I \propto Q^{-df}$. On the contrary, the intensity decay in domain I for concentrated gels tends to a Q^{-4} law characteristic of large heterogeneities (vide supra). Scanning electron micrograph views (Figure 7) show that the persistence length l_p of the fibers is very large and no real branching events can be identified in the dense mesh having zones of broader thickness typical of bundles (consistent with the SANS analysis and subsequent optical microscopy examinations). The qualification of the self-assembled fibers in **PH** and **TH** gel networks as semiflexible or rigid rodlike fibers is reasonable and introduces the most appropriate theoretical context for the analysis of the rheological properties. It is accepted that the bending rigidity of fibers generates a microscopic elastic parameter whose transduction to the macroscopic elasticity gives original and complex features that are not accounted for by the traditional rubber elasticity model.[32] In particular, the spatial distribution of the strain of the network under applied stress depends primarily on the cross-link density and fiber rigidity in regimes of affine (uniformity of the strain at different length scales) or nonaffine deformations.[33] For densely cross-linked gels, the elastic modulus G' is predicted to scale as[34]

$$G' \sim \frac{\kappa^2}{kT}\xi^{-5} \sim \frac{\kappa^2}{kT}(mC)^{5/2}\ G' \sim C^{5/2} \qquad (2)$$

κ is the bending modulus of the fibers with "monomers" of size m and concentration C. The specificity of semiflexible networks (modulus G'_{sf}) with respect to flexible (G'_f)[35] ones is illustrated

by the dependence of the elastic modulus on the mesh size (eq 3)

$$G'_{sf} \sim \frac{\kappa^2}{kT}\xi^{-2}L_e^{-3}$$

$$G'_f \sim \frac{kT}{\xi^3} \qquad (3)$$

where L_e is the mean distance between cross-links. Thus, a single microscopic length scale can describe a flexible, cross-linked gel: the mean distance ξ between cross-links. With semiflexible networks, the situation is more complex, and correlation is expected for distances longer than the mesh size. It implies that the elastic properties depend on both the mesh size and the length of the fibers. The experimental exponent 2.5 found for **PH** hydrogels agrees with the theoretical one ($^5/_2$) and thus supports the general theoretical context considered for the analysis.

The elastic modulus, yield stress, and melting temperature T_{gs} for **PH** gels were also measured as a function of the composition of the cosolvent. For a 1% w/v gel, both G' and σ^* increase with an increase of the DMSO (30−50%) content while T_g decreases linearly (Figures 8). This is surprising, since an increased amount of cosolvent in which the gelator molecules are soluble is expected to be deleterious to the integrity of the gel fibers. The apparently conflicting results question the relation between the shear elasticity of a heterogeneous network and its disintegration temperature. As the temperature is raised to T_{gs}, the solvation of the gelator molecules by DMSO is enhanced, and the collapse of the network is facilitated. On the contrary, in isothermal conditions, the increase of the shear elasticity reveals a modification of the total elastic energy available in the system. Three-dimensional SAFINs are complex networks in which the lengths of the fibers are polydisperse and their connections are not punctual and involve variable degrees of rotations of the fibers. It implies that conclusions based on simplistic models of continuum, isotropic elasticity can be very speculative. Recent theoretical models propose mechanisms generating the deformation field in semiflexible networks.[36−38] They show that the deformational properties can be much more complex than those originally assumed with rubber elasticity theories.[3,39] It is instructive to recall that in an entropic framework where thermal undulations of the fibers depend on the bending of the fibers (described by the bending modulus κ) and the work of contracting against the applied tension (described by the stretching modulus μ), the Hamiltonian of a fiber (from which the energy per unit length is derived) can be given by

$$H = \frac{1}{2}\kappa \int \mathrm{d}s\, (\nabla^2 u)^2 + \frac{1}{2}\mu \int \mathrm{d}s \left(\frac{\mathrm{d}l}{\mathrm{d}s}\right)^2 \qquad (4)$$

where s is the arc length along the undeformed fiber, $u(s)$ is the transverse displacement of the fiber, and $l(s)$ is the local extension/compression of the fiber along its undeformed contour. The degree of nonaffine strain is controlled by the ratio of the length of the fibers to a characteristic length depending on the distance between cross-links and a length over which bends in the fibers relax ($l_b = \sqrt{(\kappa/\mu)}$). Affine deformation would correspond to networks for which the energy is stored in the stretching modes of the fibers and a nonaffine regime where the energy is stored primarily in the bending of the fibers. A network becomes less affine when the bending modulus decreases or the density of cross-links decreases, and the modulus scales as $G' \sim \kappa^2$ (for densely cross-linked gels). Increased amounts of DMSO significantly increase the storage modulus and may promote an increase of the bending modulus through the implication of hydrogen bonds between the gelator aggregates and DMSO. This is equivalent to an increase of the persistence length ($l_p = \kappa/(k_B T)$) of the **PH**/DMSO fibers.

Moreover, a 1% w/v **PH** hydrogel (30% DMSO/H_2O) shows a strain-hardening phenomenon that is not found with gels in 40% and 50% DMSO/H_2O. The storage modulus varies from 5500 to ca. 9000 Pa from a strain of 0.002−0.025 (not shown). In the context of semiflexible networks, the reduction of entropy that results from the stretching of fibers is due to a depletion of the population of transverse undulation modes under extension and accounts for a nonlinear response to the stress with an entropic extension modulus that is strongly strain-hardening. A nonaffine regime has a large linear response regime while an affine entropic regime leads to a highly strain-hardening regime. According to these theoretical considerations, the **PH**/DMSO networks would evolve from an entropic affine regime at low DMSO content to a more nonaffine regime at higher DMSO contents.

SANS and optical microscopy data have shown that **TH** gels are more "crystalline" than **PH** gels. The trend is confirmed by the measurement of the transition temperature T_{gs}. It appears that the number of hydroxyl groups does not fully determine the energy of interaction between the gelator molecules or their fibers since **TH** has only four OH groups. **TH** gels melt at higher temperatures than **PH** gels while their respective crystalline solids melt at 163 and 205 °C. T_{gs} increases with the gelator concentration and decreases with an increase in the percentage of cosolvent (Figure 8). Furthermore, **PH** gels in DMSO/H_2O are thermally more stable compared to gels in EtOH/H_2O composed of a larger proportion of heterogeneities as shown by SANS. The enthalpies of disaggregation of the gels calculated from the linear plots of ln(C) versus $1/T_{gs}$ are ca. 60 and 75 kJ mol^{-1} for 30% DMSO/H_2O and 20% EtOH/H_2O, respectively. The development of heterogeneities molecularly ordered but more or less amorphous on a larger length scale is parallel with the thermal stability of the gels since the mechanical cohesiveness is then ensured by a decreasing proportion of fibers. The higher melting temperatures observed with **TH** gels can be interpreted as revealing the larger dispersion degree of the **PH** gels that contain lower fractions of large-scale heterogeneities. Indeed, it is known[40] that the size dependence of the melting temperature $T_m(r)$ of nanocrystals is of the form $T_m(r) \equiv T_0\,(1 + \alpha/r)$ with T_0 being the bulk melting temperature and α a parameter (model- and material-dependent) that can simplify to $\alpha = -2\sigma_{sl}/l_0\rho_{so}$ (l_0 being the bulk latent heat, ρ_{so} the bulk density of the solid, σ_{sl} being the solid−liquid surface tension). Although T_0 is lower for **TH** than for **PH**, the melting temperatures of the **TH** gels remain much higher than those for **PH** gels partly in relation to the increased fraction of heterogeneities.

3.4. Phase Separation in Gels. Phase separation is commonly observed for some gels derived from low mass agents and leads to the formation of microcrystals within the network anteceding, on a variable time scale, a solid−liquid phase separation. In solvent mixtures, a variation in the composition can also cause phase separation. The X-ray analysis of crystals obtained from phase-separating gels can give important clues about the molecular organization in the gel fibers and the mechanisms governing the polymorphism in gels. Crystals obtained from **PH** gels were not suitable for single-crystal analysis contrary to single crystals grown in a nongelling MeOH/CH_2Cl_2 solution,

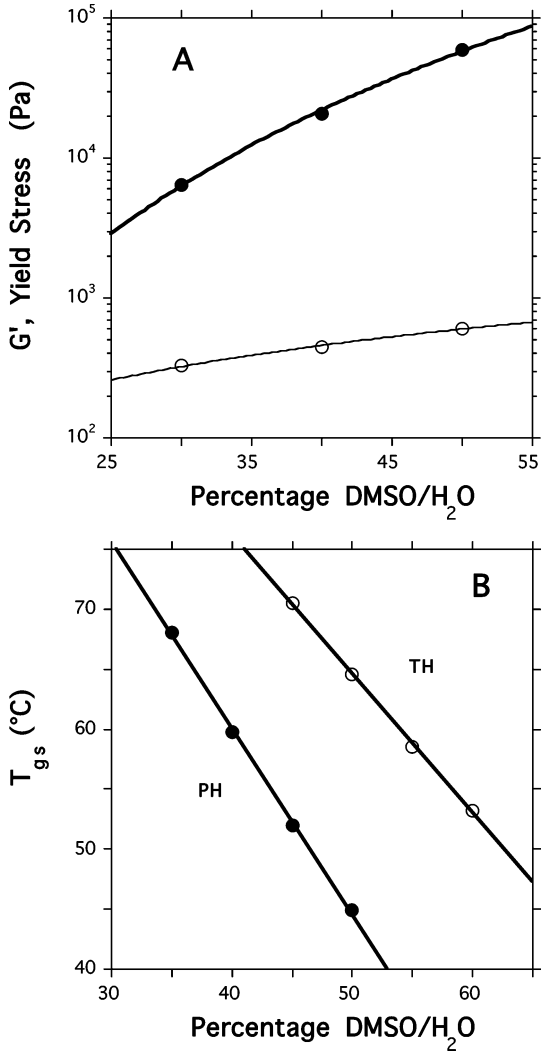

Figure 8. (A) Dependence of G' (●) and yield stress (○) with the DMSO content in **PH** hydrogels ($C = 1.0\%$ w/v). (B) Variation of the gel melting temperature T_{gs} for **PH** and **TH** systems ($C = 0.4\%$ w/v) as a function of DMSO/H_2O.

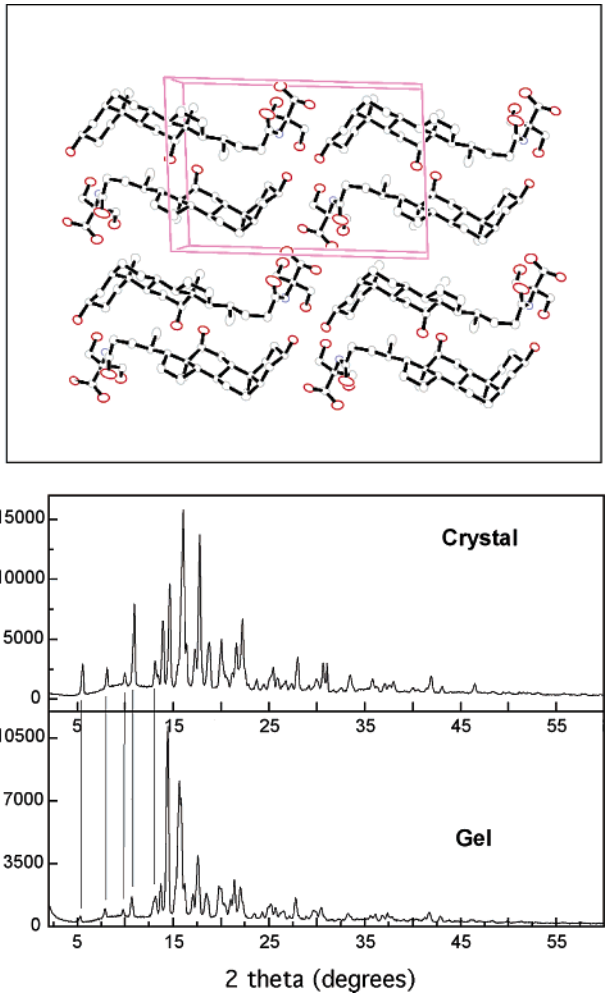

Figure 9. Top panel: **PH** molecular packing in the $P2_1$ monoclinic space group. Head-to-tail sequences are observed in the (a,c) plane. Bottom panel: WAXS pattern of **PH** single crystals grown from a nongelling MeOH/CH_2Cl_2 solution. Monoclinic space group: $P2_1$, $a = 11.0890$ Å, $b = 7.2579$ Å, $c = 16.3294$ Å. $\alpha = \gamma = 90.00°$, $\beta = 93.60°$, $Z = 2$. The lower diffraction pattern is that for a **PH** xerogel powder from a 1.5% w/v gel in 40% DMSO/H_2O.

which provide the reference morph of the **PH** gelator. The molecules form a head-to-tail bilayer structure in each layer of a monoclinic arrangement ($P2_1$ with $Z = 2$) as shown in Figure 9. The layers run antiparallel with respect to each other, and the hydrophobic α-faces of the steroid backbones associated by van der Waals interactions are segregated from the hydrophilic β-faces that are sequestered together. Channels are formed where extensive hydrogen-bonding interactions connect neighboring molecules through N−H, C═O, and hydroxyl groups. The amide carbonyl and side chain hydroxyl groups are also internally hydrogen-bonded. The head-to-tail structure is also found in the gel fibers as shown by the SANS analysis. It suggests that molecular arrangements in the single crystals and the xerogel are similar, and the assumption is also supported by the related powder X-ray diffraction patterns that exhibit Bragg peaks at very similar positions, especially at low angles (Figure 9).

Optical birefringent textures of **PH** and **TH** hydrogels can provide useful information about the orientation correlations between the fibers at a micron scale. Lyotropic microdomains can act as precursors for further evolutions of the network texture and thus are important pieces of information to analyze the metastability of gels. Figure 10 illustrates the various situations encountered with **PH** and **TH** hydrogels. A **PH** gel (40% DMSO/H_2O) shows no texture at 0.3% w/v, a weak one at 0.75% w/v, and a stronger one at 1.3% w/v. **TH** gels have stronger textures than those of **PH**. Consistently, SANS data have pointed to the greater proportion of large heterogeneities in the **TH** gels at all concentrations compared to **PH** gels, consistent with the visual aspect of the gels. Maltese crosses are also observed and characterize the presence of spherulitic domains grown from a central nucleating site. After aging, birefringent needlelike crystals have grown in the network at the expense of the spherulitic nodes, eventually leading to a phase separation process. The spherulitic crystals have needlelike branches emerging from a nodal point (or nucleation site). Similar crystals are obtained from phase-separated **TH** gels. The shape of the crystals obtained in a nongelling mother solution is quite different and appears as flat needles. With spherulitic growth, there is no relationship between the crystallographic planes and the direction of growth by contrast to dendritic growth that leads to a dense fibrillar mesh. The electron micrograph of Figure 7 shows a "Mikado-like" distribution of fibers, and branching does not seem to be a characteristic feature of these gels. More likely, homogeneous nucleation leads to the random growth of fibers with a high space-filling power. Various nucleation events may still occur during the kinetics

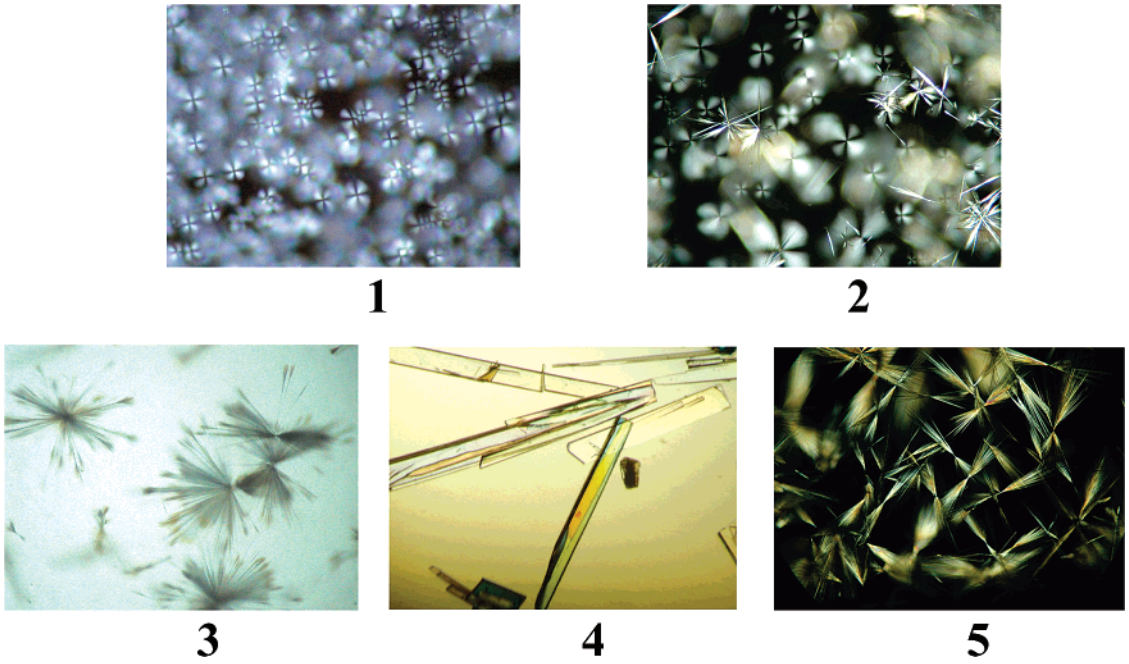

Figure 10. Optical microscopy (crossed polarizers) in 0.5 mm quartz cells. **1**: **PH** gel (C = 1.2% w/v) in 40% DMSO/H_2O. **2**: **TH** gel (C = 0.45% w/v) in 50% DMSO/H_2O (1 h after preparation). **3**: **PH** crystals grown from a gel (C = 0.8%) in 25% EtOH/H_2O. **4**: Crystals grown from a nongelating MeOH/CH_2Cl_2 mixture. **5**: Crystals obtained from a **TH** gel (C = 1% w/v) in 50% DMSO/H_2O.

of aggregation of the system along at least two possible mechanisms. First, a double nucleation mechanism can use the surface of a preexisting fiber to develop a new fiber growing attached to the parent fiber in a nonspecified orientation and so ultimately generates a dense network via a highly autocatalytic process.[41] Second, spherulitic domains, as observed by polarizing microscopy, are higher-order assemblies that may result from aging or incubation at higher temperatures while heterogeneous impurities can also serve as cores causing the formation of the radial pattern of growing spherulites. It has been shown in networks of molecular organogels with a cholestan-naphthylcarbamate derivative[42] that the incubation temperature is a determinant of the spherulitic versus fibrillar (low T) growth competition. Optical micrographs of Figure 10 recorded at two aging times for a phase-separating **TH** gel in DMSO/H_2O confirm that crystal growth develops on the preexisting crystalline seeds of the spherulites toward phase separation of the metastable gels. This sequence of morphological variations might be a general pattern for other SAFINs in molecular gels. It is noteworthy that the presence of spherulitic domains, in significant proportions for **TH** gels, certainly affects the viscoelastic properties in a complex manner. To minimize such an influence (not taken into account in the considered theoretical models), the analysis of the rheological scaling law of Figure 6 was conducted for **PH** gels only.

4. Conclusion

In the present work, the gel networks formed with neutral bile derivatives in aqueous solutions of various polar cosolvents have been characterized. The study has focused on two highly hydroxylated derivatives differing only by one OH group. The structure of the fibers that composes the networks was determined by SANS. The cylindrical fibers are rigid with diameters of 92 Å (**PH**) and 79 Å (**TH**) and exhibit monodisperse sections. From absolute intensity measurements (Table 1), the average value of $n_L \approx 5$ molecules $Å^{-1}$ shows that **PH** gels in DMSO/D_2O have fibers with $5 \times 5 = 25$ molecules aggregated per cross-sectional unit (assuming a mean axial stacking period of ca. 5.0 Å). It corresponds to a schematic picture of a circular cross-section with four diameters involving six aggregated molecules each. In alcoholic mixtures, the aggregation number decreases to ca. 12 molecules corresponding to 3 diameter lines with 4 molecules each in thinner fibers (79 Å). For **TH** fibers (ca. 80 Å diameter) the integral of the invariant calculation has no Bragg peak included, and the crossover between Q-domains I and II occurs at lower angles compared to **PH** in the alcoholic mixture. The proportion of heterogeneities is more than twice that for **PH** gels at similar concentrations. For **PH** gels, compact bundles are revealed by a Bragg peak while **TH** gels are less stable and contain more amorphous junction zones. A change in the nature of the cosolvent (from DMSO/D_2O to CD_3CD_2-OD) can considerably enhance the proportion of nodal zones in **PH** gels by a factor of 3. Such evaluations have been made possible by the elaboration of a SANS methodology using scattering invariants with favorable experimental scattering curves that separate the scattering component for the fibers and the heterogeneities of the networks. This is the first time that such a simple method can provide the volume fraction in a network and allow all corrections for refined calculations of the number of gelator molecules really involved in the fibrillar structures.

Rheological features and in particular the scaling law of the shear elasticity versus concentration can be well described in the context of semirigid networks presenting a thermal distribution of transverse undulations. Simple calculations from SANS data estimate a mean mesh size of ca. 500 Å (at $C \approx 0.013$ $g.cm^{-3}$) for **PH** gels and support the hypothesis that the persistence length of the fibers is much larger than the mesh size. This is also supported by a scanning electron microscopy view that shows a mat of Mikado-like distributed fibers where no real branching events can be discerned. The elasticity of such networks depends on a balance between the stretching and bending moduli in a system whose deformation field can be more or less affine. With added DMSO, strain-hardening effects are observed at low contents, while at higher DMSO concentra-

tions the bending rigidity is enhanced through a chelating-like hydrogen-bonding process and the networks become more nonaffine.

Wide-angle X-ray scattering (WAXS) measurements suggest that the molecular arrangements in single crystals obtained in nongelling conditions and in gel fibers are about identical. Optical microscopy suggests that orientation correlations are present in the SAFINs at a micron scale that are likely due to the formation of bundles most probably through heterogeneous double nucleation mechanisms that qualitatively account for the autocatalytic character of the kinetics of aggregation.

The texture of the networks appears complex and depends on the concentration of the gelator (number density of fibers), the type and concentration of cosolvent (affine degree of the network) and aging of the system. The network is a mesh of randomly distributed rigid fibers decorated with birefringent merging zones (bundles) that use preexisting rodlike fibers as stakes for subsequent fibrillar growth. A coexistence with spherulitic microdomains is also observed to be at the origin of the phase separation "parasitic" phenomenon. Slow rearrangements toward crystallites appear to germinate at the spherulitic seeds. SANS has shown to be a suitable tool to extract the proportion of large-scale heterogeneities in the network (and so that of fibers) but cannot distinguish their internal texture. Nevertheless, the isotropic character of the neutron scattering indicates that the resultant of oriented microdomains mainly formed with bundles is random on a nanoscale (mosaic effect) while no anisotropy is expected from the growth of spherulitic domains. Such network architecture and evolution of its components with aging are thought to be very common in metastable molecular gels.

Acknowledgment. The present work was supported by the Indo-French Center for Promotion of Advanced Research (IFCPAR Project No. 2605-1), which is deeply thanked. Institut Laue Langevin (ILL, Grenoble, France) is acknowledged for providing access to the spectrometer and all technical support. Dr. Bruno Demé (ILL) is thanked for his valuable help during the neutron experiments, and we are grateful to Dr. A. R. Choudhury and Suvadeep Nath for providing the X-ray analysis of the **PH** solids.

References and Notes

(1) *Molecular Gels: Materials with Self-Assembled Fibrillar Networks*; Weiss, R. G., Terech, P., Eds.; Springer: Dordrecht, The Netherlands, 2006.

(2) Liu, X. Y. In *Low Molecular Mass Gelators*; Fages, F., Ed.; Topics in Current Chemistry 256; Springer: Dordrecht, The Netherlands, 2005; p 1.

(3) Flory, P. *Principles of Polymer Chemistry*; Cornell University Press: Ithaca, NY, 1953.

(4) Lin, Y.-C.; Kachar, B.; Weiss, R. G. *J. Am. Chem. Soc.* **1989**, *111*, 5542.

(5) Murata, K.; Aoki, M.; Susuki, T.; Harada, T.; Kawabata, H.; Komori, T.; Ohseto, F.; Ueda, K.; Shinkai, S. *J. Am. Chem. Soc.* **1994**, *116*, 6664.

(6) Hishikawa, Y.; Sada, K.; Watanabe, R.; Miyata, M.; Hanabusa, K. *Chem. Lett.* **1998**, 795.

(7) Willemen, H. M.; Vermonden, T.; Marcelis, T. M.; Sudhlter, E. J. R. *Langmuir* **2002**, *18*, 7102.

(8) Maitra, U.; Kumar, P. V.; Chandra, N.; D'souza, L. J.; Prasanna, M. D.; Raju, A. R. *J. Chem. Soc., Chem. Commun.* **1999**, 595.

(9) Maitra, U.; Mukhopadhyay, S.; Sarkar, A.; Rao, P.; Indi, S. S. *Angew. Chem., Int. Ed.* **2001**, *40*, 2281.

(10) Wade, R. H.; Terech, P.; Hewat, E. A.; Ramasseul, R.; Volino, F. *J. Colloid Interface Sci.* **1986**, *114*, 442.

(11) Terech, P.; Ramasseul, R.; Volino, F. *J. Phys. Fr.* **1985**, *46*, 895.

(12) Terech, P.; Ramasseul, R.; Volino, F. *J. Colloid Interface Sci.* **1983**, *91*, 280.

(13) Sobotka, H.; Czeczowiczka, N. *J. Colloid Sci.* **1958**, *13*, 188.

(14) Rich, A.; Blow, D. M. *Nature* **1958**, *46*, 423.

(15) Maitra, U.; Babu, P. *Steroids* **2003**, *68*, 459.

(16) Sangeetha, N. M.; Bhat, S.; Choudhury, A.; Maitra, U.; Terech, P. *J. Phys. Chem. B* **2004**, *108*, 16056.

(17) Sangeetha, N. M.; Balasubramanian, R.; Maitra, U.; Ghosh, S.; Raju, A. R. *Langmuir* **2002**, *18*, 7154.

(18) Samuel, R. E.; Salmon, E. D.; Briehl, R. W. *Nature* **1990**, *345*, 833.

(19) Institut Laue Langevin Homepage. http://www.ill.fr.

(20) Debye, P.; Bueche, A. M. *J. Appl. Phys.* **1949**, *20*, 518.

(21) Schaefer, D. W.; Keefer, K. D. *Phys. Rev. Lett.* **1986**, *56*, 2199.

(22) Teixeira, J. *J. Appl. Crystallogr.* **1988**, *21*, 781.

(23) Terech, P. Small-angle scattering and molecular gels. In *Molecular Gels: Materials with Self-Assembled Fibrillar Networks*; Weiss, R. G., Terech, P., Eds.; Springer: Dordrecht, The Netherlands, 2006.

(24) Hukins, D. W. L. *X-ray Diffraction by Disordered and Ordered Systems*; Pergamon Press: Oxford, U. K., 1981.

(25) Wu, H.; Morbidelli, M. *Langmuir* **2001**, *17*, 1030.

(26) Terech, P.; Pasquier, D.; Bordas, V.; Rossat, C. *Langmuir* **2000**, *16*, 4485.

(27) Brinksma, J.; Feringa, B. L.; Kellog, R. M.; Vreeker, R.; Van Esch, J. *Langmuir* **2000**, *16*, 9249.

(28) Jones, J. L.; Marques, C. M. *J. Phys. Fr.* **1990**, *51*, 1113.

(29) Gibson, L. J.; Ashby, M. F. *Cellular Solids: Structure and Properties*; University Press: Cambridge, U. K., 1997.

(30) Leon, E. J.; Verma, N.; Zhang, S.; Lauffenburger, D. A.; Kamm, R. D. *J. Biomater. Sci., Polym. Ed.* **1998**, *9*, 297.

(31) Shih, W.-H.; Shih, W. Y.; Kim, S.-I.; Liu, J.; Aksay, I. A. *Phys. Rev. A* **1990**, *42*, 4772.

(32) Rubinstein, M.; Colby, R. H. *Polymer Physics*; Oxford University Press: London, 2003.

(33) Head, D. A.; Levine, A. J.; Mackintosh, F. C. *Phys. Rev. Lett.* **2003**, *91*, 108102.

(34) Macintosh, F. C.; Käs, J.; Janmey, P. A. *Phys. Rev. Lett.* **1995**, *75*, 4425.

(35) De Gennes, P. G. *Scaling Concepts in Polymer Physics*; Cornell University Press: Ithaca, NY, 1979.

(36) Head, D. A.; Levine, A. J.; Mackintosh, F. C. *Phys. Rev. E* **2003**, *68*, 061907.

(37) Levine, A. J.; Head, D. A.; Mackintosh, F. C. *J. Phys.: Condens. Matter* **2004**, *16*, S2079.

(38) Wilhelm, J.; Frey, E. *Phys. Rev. Lett.* **2003**, *91*, 108103.

(39) Doi, M.; Edwards, S. F. *The Theory of Polymer Dynamics*; Clarendon: Oxford, U. K., 1986.

(40) Unruh, K. M.; Sheehan, J. F.; Huber, T. E.; Huber, C. A. *Nanostruct. Mater.* **1993**, *3*, 425.

(41) Ferrone, F. A.; Hofrichter, J.; Eaton, W. A. *J. Mol. Biol.* **1985**, *183*, 611.

(42) Huang, X.; Terech, P.; Raghavan, S. R.; Weiss, R. G. *J. Am. Chem. Soc.* **2005**, *127*, 4336.